Sensor and Simulation Notes

Note 444

April 2000

An Improved Collapsible Impulse Radiating Antenna

Leland H. Bowen and Everett G. Farr
Farr Research, Inc.

William D. Prather
Air Force Research Laboratory, Directed Energy Directorate

Abstract

We continue here the development of a Collapsible Impulse Radiating Antenna (CIRA), which is compact, lightweight, and man-portable. In Sensor and Simulation Note 440, we described the design, fabrication and testing of two 1.22 m (48 in) diameter collapsible antennas. The first antenna is called a Collapsible IRA, or CIRA. The second antenna had expansion seams in the reflector to provide a multifunction or adjustable beamwidth capability. This antenna was called a Collapsible Multifunction IRA, or CMIRA. In this paper we describe design changes for the CIRA which reduce the size, weight and wind resistance of the antenna. The paraboloidal shape of the reflector was also improved, thereby improving the RF characteristics of the antenna. The multifunction capability was not included in the current design, however, it could be added later to create an improved MIRA. We tested the antenna using standard time domain antenna range techniques, and converted the results to IEEE standard gain in the frequency domain. The modified CIRA is usable from below 50 MHz to above 8 GHz. The FWHM of the normalized impulse response is 73 ps.

This work was funded in part by the Air Force Office of Scientific Research, Alexandria, VA, and in part by the Air Force Research Laboratory, Directed Energy Directorate, under contract number F29601-98-C-0004.

I. Introduction

We continue here our development of the Collapsible Impulse Radiating Antenna (CIRA). The improvements described here result in a lighter, more compact version of the antenna with improved RF characteristics, lower wind loading, and improved mechanical ruggedness.

In [1], we developed antennas that were collapsible and portable, and had an adjustable beamwidth. The design we selected resembles an umbrella, with a reflector and feed arms sewn from conductive and resistive fabric. We built two versions of the antenna that were similar, the difference being that the first version did not have the adjustable beamwidth or multifunction capability. Therefore, the first version was called the Collapsible IRA, or CIRA. The second version had expansion seams in the reflector to allow the surface curvature to be adjustable. This antenna was called the Collapsible MIRA, or CMIRA.

The designs of both the CIRA and CMIRA were based on a 1.22 m (48 in) diameter parabolic dish with a focal length of 0.488 m (F/D = 0.4). The reflectors for these two antennas were constructed from conductive rip-stop nylon. The use of conductive fabric on an umbrella type frame provided a very good reflector that met the requirements for a man-portable MIRA. However, several problems were encountered, such as stretch in the fabric, high wind loading, and difficulty in opening the antennas. In this paper we describe the design changes implemented to alleviate the problems. The continued development of a collapsible, man portable IRA has focused on the CIRA. The main changes are the use of a very tough conductive mesh fabric in place of the rip-stop nylon and redesign of the mechanism for locking the antenna in the open position. The new fabric greatly reduced the wind loading and improved the dimensional stability of the reflector. The new locking mechanism is much easier to use and eliminated possible error in setting up the antenna. Also, the number of panels was reduced from 20 to 12, which reduced the size and weight of the CIRA. Finally a nose piece was added at the focus of the reflector, to add mechanical strength and to protect the delicate electrical connections located there.

We measured the characteristics of the modified antenna using the time domain outdoor antenna range of Farr Research. The time domain data were processed to obtain the normalized impulse response as described in [2]. We made pattern measurements at 2.5° intervals in both the H and E planes and converted them to IEEE standard gain. The conversion from impulse response to IEEE standard gain is based on the derivation in Section III of [1]. We present the impulse response characteristics in both the time and frequency domains. We also present the standard gain on boresight as a function of frequency. Finally, we present the standard gain as a function of angle in the principal planes, at multiple constant frequencies.

II. Data Acquisition System and Sensor Calibration

We provide now the details of the data acquisition system and the test setup. The data acquisition system used here was the same as that used in [1], with the minor exception that a different TEM sensor was used. In [1] we used a 100 Ω sensor that was a prototype of the TEM-2-100 used for the current measurements. Here, we used a final version of the TEM-2-100 sensor (large, 100 ohms), and the TEM-1-50 sensor (small, 50 ohms). Therefore, we provide here calibration data for both sensors, using the techniques of [1]. Both of these sensors can be described as essentially a half TEM horn mounted against a truncated ground plane.

The TEM-2-100 sensor is pictured in Figure 2.1. This TEM horn is a 100 Ω sensor with a ground plane that measures 20 x 48 inches. The TDR of the sensor is shown in Figure 2.2. Two identical TEM sensors were used to calibrate the sensor using the techniques of [2]. The calibration was performed with the sensor apertures 20 m apart and 3.0 m above the ground. This provides a delay of 3.0 ns before the ground bounce signal arrives.

The calibration of the TEM-2-100 sensor is provided in Figures 2.3 – 2.6. We truncated the signal at the receiving sensor shortly after the impulse to remove the ground bounce. Also, we zero-padded the signal out to 20 ns for processing, to improve the low frequency response. We show these modifications in Figure 2.3. The normalized impulse response has a FWHM of 50 ps as shown in Figure 2.4. The frequency response is extremely flat as shown in Figures 2.5 – 2.6. This sensor has a clear time of 4 ns and a maximum gain of about 17 dB. The 100 Ω impedance of this antenna increases the sensitivity, due to the increased effective height, but causes a mismatch into 50 Ω cables. However, the improved sensitivity more than offsets the effect of the mismatch.

Next, we show the TEM-1-50 sensor in Figure 2.7. This sensor has a 50 Ω impedance to match 50 Ω cables. The ground plane for this sensor measures 10 x 24 inches. The TDR of the sensor is shown in Figure 2.8. As above, two identical TEM sensors were used to calibrate the sensor using the techniques of [2]. The calibration was performed with the sensor apertures 10 m apart and 3.0 m above the ground. This provides 5.5 ns delay before the ground bounce signal arrives.

The calibration of the TEM-1-50 sensor is provided in Figures 2.9 – 2.12. No truncation or zero padding of the signal was required. The normalized impulse response has a FWHM of 31 ps as shown in Figure 2.10. The frequency response is extremely flat as shown in Figures 2.11 – 2.12. This sensor has a clear time of 2 ns and a maximum gain of approximately 15 dB.

Figure 2.1. FRI-TEM-02-100 sensor.

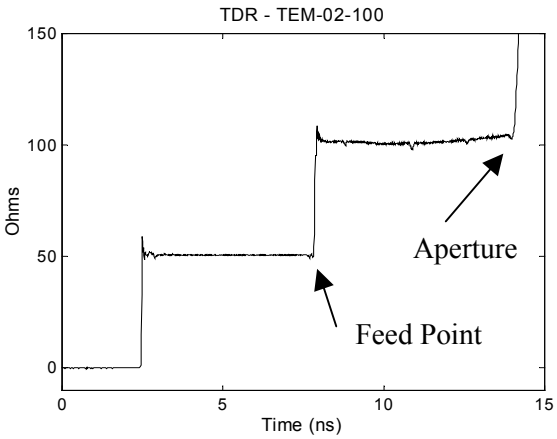

Figure 2.2. TDR of the FRI-TEM-02-100.

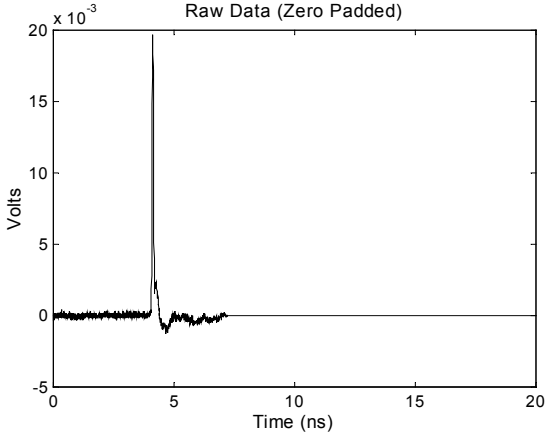

Figure 2.3. FRI-TEM-02-100 raw data.

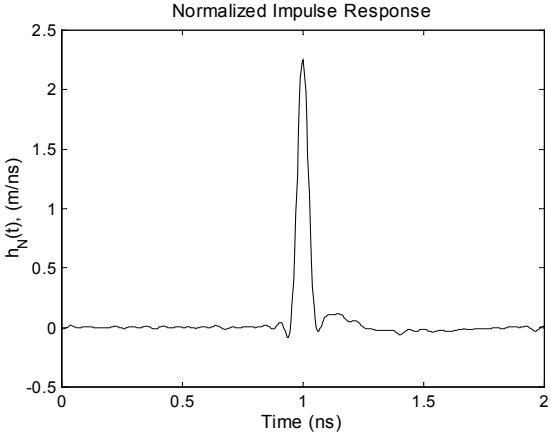

Figure 2.4. Normalized impulse response.

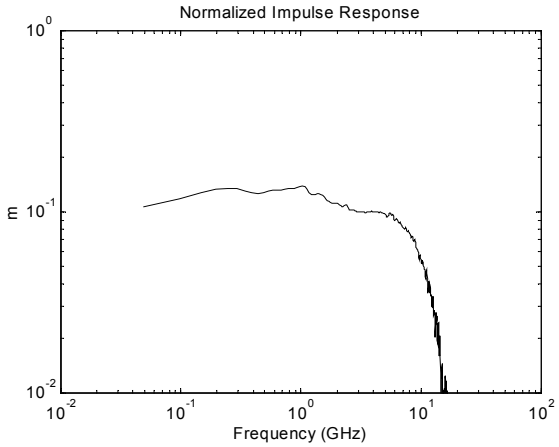

Figure 2.5. Normalized impulse response.

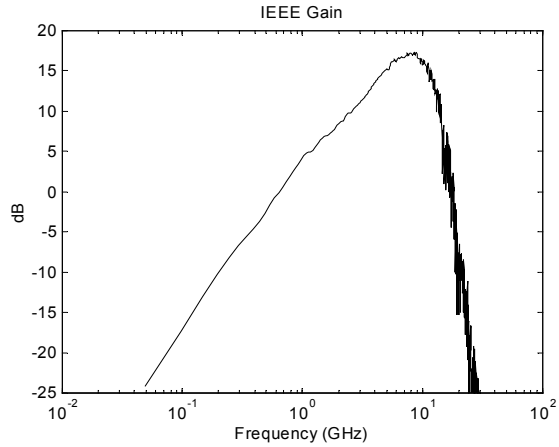

Figure 2.6. IEEE standard gain.

Figure 2.7. FRI-TEM-01-50 sensor.

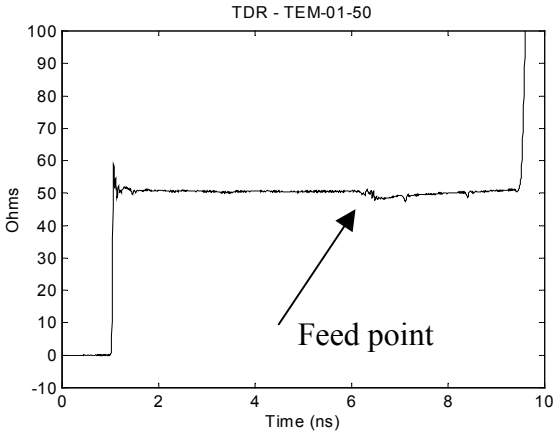

Figure 2.8. TDR of the FRI-TEM-01-50.

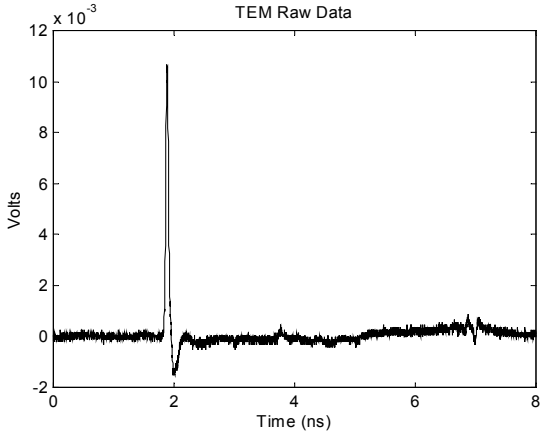

Figure 2.9. FRI-TEM-01-50 raw data.

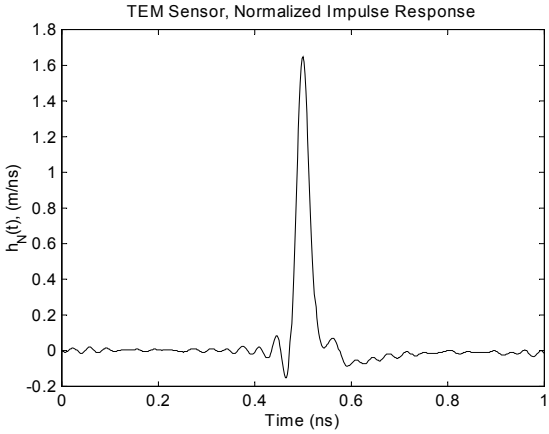

Figure 2.10. Normalized impulse response.

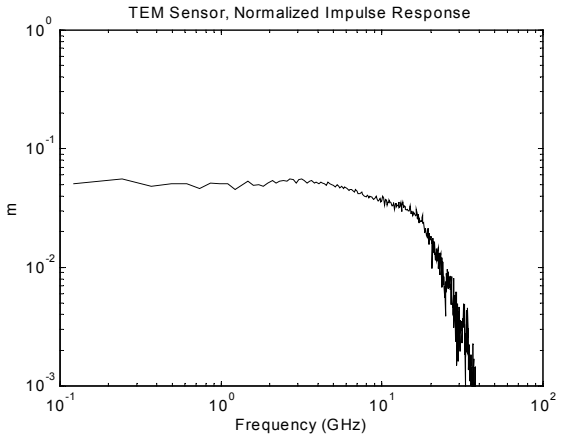

Figure 2.11. Normalized impulse response.

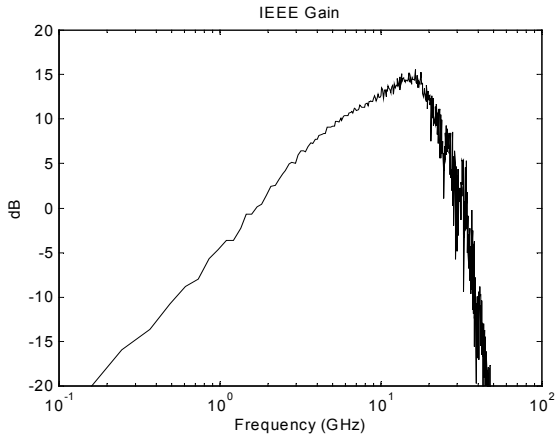

Figure 2.12. IEEE standard gain.

III. CIRA Modifications and Fabrication

We provide here a brief overview of the design of the CIRA, and we describe the new modifications. This extends the previous descriptions of the CIRA and CMIRA in [1]. The CIRA is designed to open and close like an umbrella. The parabolic reflectors are 1.22 m (48 in.) in diameter with F/D = 0.4. The reflectors are constructed from conductive fabric supported on a frame of fiberglass rods attached to an aluminum center housing by aluminum pivots or hinges. The feed arms are made from a combination of conductive and resistive fabrics. The splitter was provided by Prodyn Technologies. It consisted of a 50 Ω input impedance connector, which then splits into two 95 Ω cables. The cables attach to the feed arms at the feed point in a series/parallel configuration as standard for IRAs with 4 feed arms.

We redesigned the collapsible antenna to include a large number of modifications and improvements. The cross section of the new CIRA is shown in Figure 3.1. The changes include reducing the diameter of the collapsed antenna by decreasing the number of stays (or panels) from 20 to 12. This allow us to reduce the diameter of the can that supports the antenna and holds the RF splitter. The collapsed antenna now measures 102mm (4 in.) diameter x 81 cm (32 in.) long. The antenna weighs 2 kg (4.5 lb.). Reducing the number of stays also reduced the shadowing of the reflector. The variation from the desired paraboloid with 12 panels is about ±10mm as measured from the focal point. It was found that variations in the shape of the reflector cause severe degradation of the impulse response and the beam shape. The original CIRA and CMIRA as built were too flat, and were therefore somewhat out of focus. This problem was caused by stretch in the rip-stop nylon fabric of the dish and by small variations in the cutting and sewing of the panels. This problem was addressed with improved patterns for the fabric, greater quality control, and better sewing techniques.

A number of additional modifications were made to the CIRA. The catch mechanism that holds the dish open was modified to greatly improve the ease of operation. Fewer more flexible stays reduce the force required to open the antenna. The center shaft has been modified to increase rigidity. A protective nose piece has been fitted over the apex of the antenna, to provide mechanical support, and to protect the delicate electrical connections located there. The rip-stop nylon in the reflector has been replaced with a very tough mesh fabric, to reduce wind loading and improve dimensional stability of the parabolic dish. At first we tried to use the same mesh fabric for the feed arms. However, tests showed that the rip-stop nylon provided a flatter TDR and better overall antenna performance. The present version, which has only a focused configuration, is constructed of a combination of the mesh and rip-stop nylon fabrics. The mesh fabric is a silver and nickel plated material with a resistance of less than 0.2 Ω/square. The air permeability of this fabric is approximately 19.3 $(m^3/s)/m^2$ or 3800 $(ft^3/min.)/ft^2$.

This version of the CIRA is now commercially available from Farr Research. It has been designated as model FRI-CIRA-1. We show the new version with the conductive mesh fabric for the dish and rip-stop nylon for the feed arms in Figures 3.1 – 3.3. Note that the mesh material is somewhat “see through” or transparent, which reduces visibility of the antenna to some extent. Wind conditions during testing at the Farr Research outdoor antenna range confirmed that the mesh fabric greatly reduces wind loading on the parabolic dish antenna.

The antenna is provided with several means of support, as shown in Figure 3.3. First, a lightweight carbon fiber tripod with a ball head is provided as the main means of support. This tripod with head weighs less than 2.3 kg (5 lb.), and it has a hook for attaching a sandbag, for added stability in high wind conditions. In addition, a multipurpose clamp is provided, that can be used to attach the CIRA to a variety of fixed objects, such as trees and fences. The ball head is also used with the clamp for positioning and aiming the antenna as shown in Figure 3.2. Finally, loops are provided on the back of the antenna for the attachment of ropes. This makes it possible to raise the antenna into a tree and aim it in a given direction using ropes.

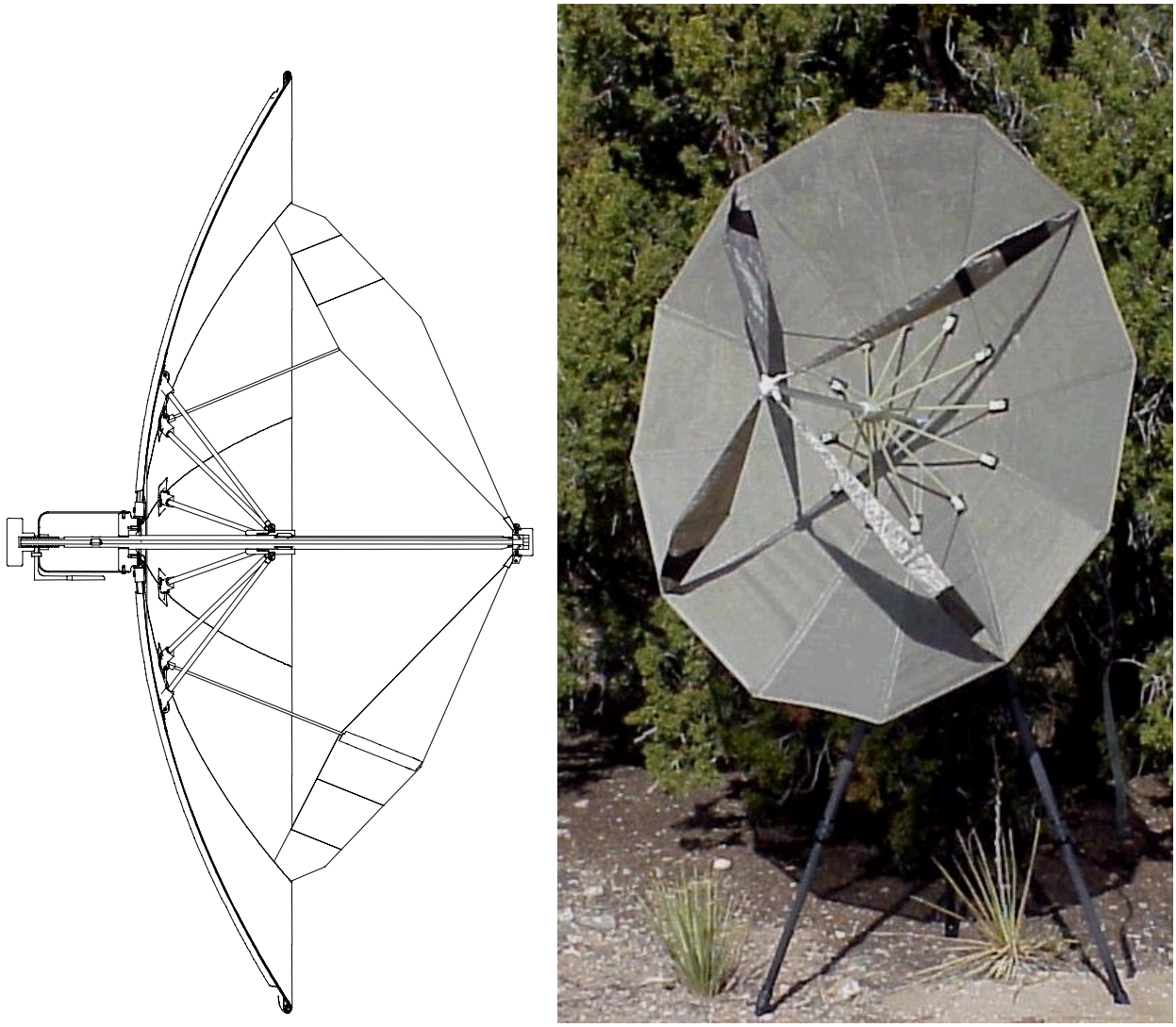

Figure 3.1 CIRA cross section and antenna mounted on lightweight tripod.

Figure 3.2 Back side of CIRA mounted on tripod (left) and clamp (right).

Figure 3.3 CIRA collapsed for carrying with support accessories.

IV. CIRA Data

We measured the characteristics of the CIRA-1 using the time domain outdoor antenna range of Farr Research. Both the TEM-2-100 and TEM-1-50 horn sensors were used for these measurements, as described in Section II. At first, we had planned on using just the larger sensor, in order to obtain the best possible low-frequency measurement. We later added the measurements with the smaller sensor, in order to be sure that we could observe the fastest possible FWHM out of the CIRA. A Picosecond Pulse Labs 4015C step generator was used to drive the TEM horn antennas. This step generator has a 4 V output with a 25 ps risetime. The response of the CIRA-1 was recorded using a Tektronix 11801B Digital Sampling Oscilloscope. The test setup is described more fully in [1]. The distance between the antennas was 20 m and the height was 3 m. Antenna pattern measurements in the H and E planes were made at 2.5° increments. Also, the IEEE standard gain is computed and plotted on boresight as a function of frequency and at various frequencies as a function of angle in the principal planes.

The test data for the CIRA-1 with the new umbrella are as follows. The TDR of the antenna is shown in Figure 4.1. The TDR at the feed point and the feed arms is the best we have achieved on this type antenna. In Figures 4.2 – 4.7 we show the on-boresight characteristics of the CIRA-1 as measured using the TEM-2-100 sensor on the left and the TEM-1-50 sensor on the right. For the larger sensor (TEM-2-100) the data were clipped just before the arrival of the ground bounce signal and then zero padded out to 20 ns, to provide frequency information down to 50 MHz. No modifications were made to the data from the small sensor (TEM-1-50). It is interesting to note that the measurements using the two sensors are almost identical. The FWHM of the normalized impulse response (Figure 4.3) is 73 ps when measured with the larger sensor and slightly smaller (68ps) when measured with the smaller sensor. The CIRA proved to be usable from below 50 MHz to above 8 GHz, as shown in Figures 4.4 and 4.5. After seeing the results using the large sensor, we had hoped that the smaller sensor would show an even better high-frequency response, but the results are quite similar.

When deciding the distance at which to place the sensor, one has to realize that the far-field begins at a distance that is dependent upon the smallest FWHM one expects to measure. We expected a FWHM of around 100 ps, so we expected that a distance of 20 meters would be adequate. However, we were pleasantly surprised by the 70ns FWHM measurements of the improved CIRA. This faster impulse width extends the far field to around 25m, using the formula $r > (3/2)a^2/(c\,t_{FWHM})$, where a is the antenna radius, c is the speed of light in free space, and t_{FWHM} is the FWHM of the radiated impulse response. While there was no opportunity to make new measurements at a greater distance, we believe the error in the measurement is small.

Next, we provide the gain vs. frequency in Figure 4.5. This data shows that at lower frequencies the response of this antenna is somewhat flatter than previous measurements and the high-frequency response is approximately smooth to 8 GHz. The peak gain of the CIRA is 23 dB at 4 GHz. We find the h_a of the antenna from the integral of the impulse response in Figures 4.6 – 4.7 to be 0.30 m, so the midband effective height of the antenna is 15 cm. This value for h_a is 76 % of the theoretical value of 0.396 m given in [1,2].

In Figure 4.8 we show the cross polarization (crosspol) response of the CIRA. The IEEE gain on boresight for the crosspol case is shown in Figure 4.9. The crosspol response is 10 – 20 dB below the copol response from Figure 4.5. This data may be of interest due to recent work suggesting improvements in the IRA that would result in improved gain and reduced crosspol [4]. This is accomplished by placing the feed arms at ±30º from vertical, instead of ±45º, which we currently have in the CIRA. Since each panel of the CIRA is 30° wide, it should be straightforward to incorporate the new feed arm positions into the CIRA, but the principle has yet to be demonstrated experimentally.

In Figures 4.10 – 4.11 we show the principal plane pattern cuts of the antenna at various frequencies. Next, in Figures 4.12 – 4.15 we show the antenna pattern in the H and E planes, based on the peaks of the raw voltage measurements. Note that as the antenna turns on the tripod, the peak field can shift in time with our tripod mounting, and we have made no attempt to adjust the time delay in our raw data to compensate for this. The half voltage beamwidth is 5.1° in the H plane and 6° in the E plane. If we choose to use the half power beamwidth, we have ~3° in both the H and E planes.

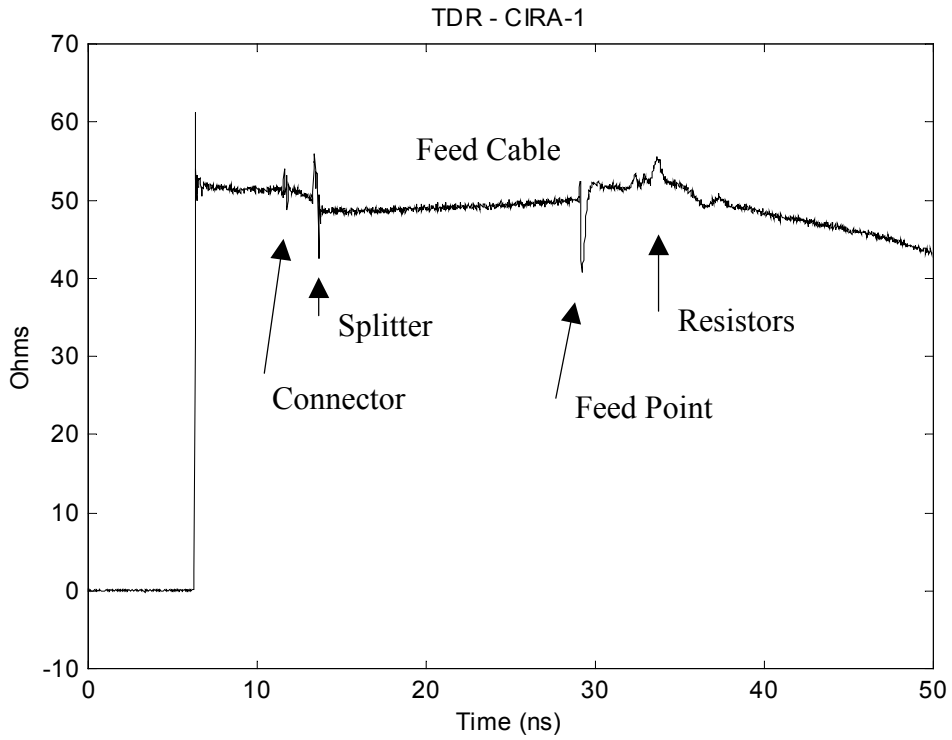

Figure 4.1 TDR of CIRA.

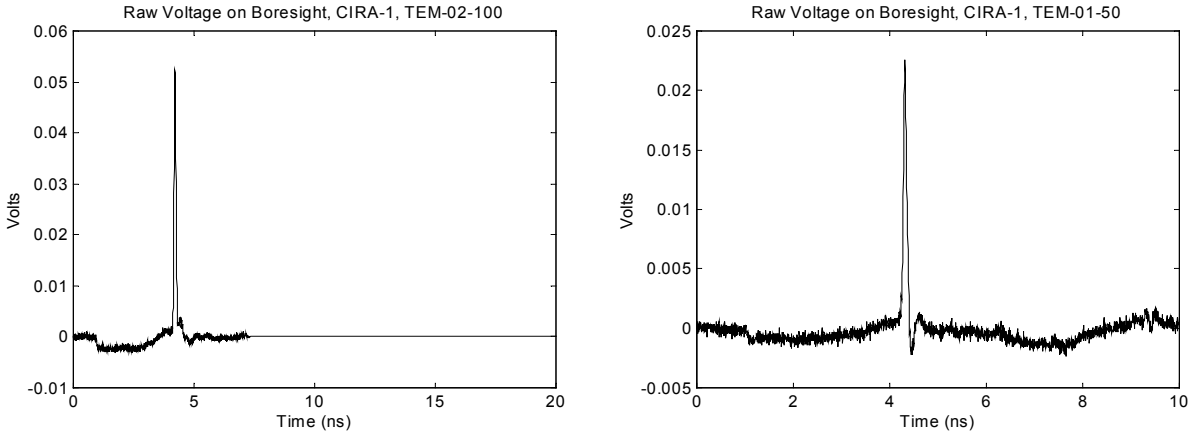

Figure 4.2 Raw data on boresight with ground bounce removed and zero-padded.

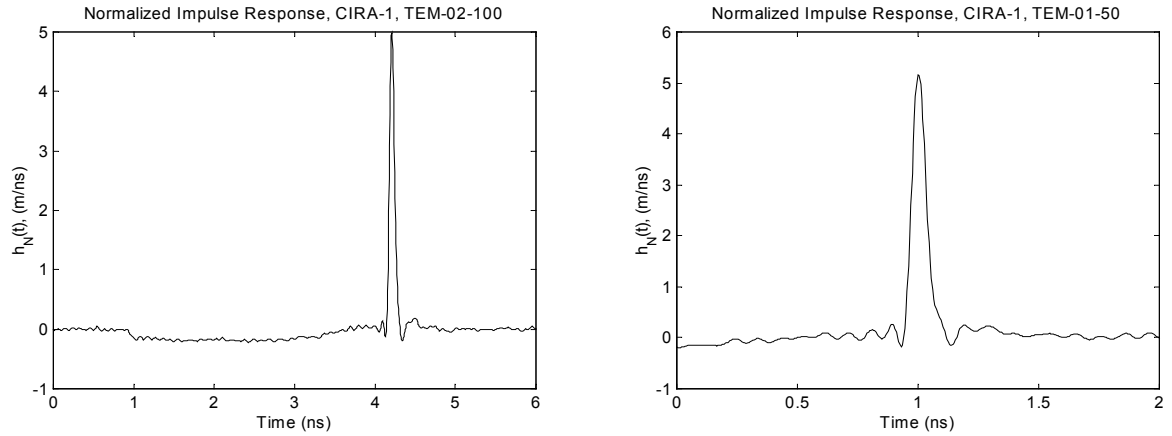

Figure 4.3 Expanded normalized impulse response [2] (FWHM = 73 ps, left, 68 ps, right).

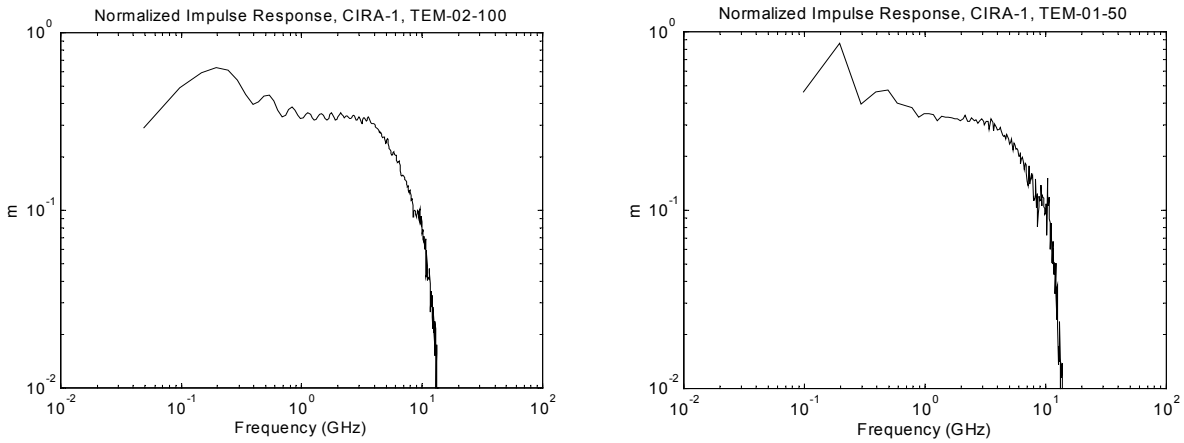

Figure 4.4 Normalized impulse response of the CIRA on boresight.

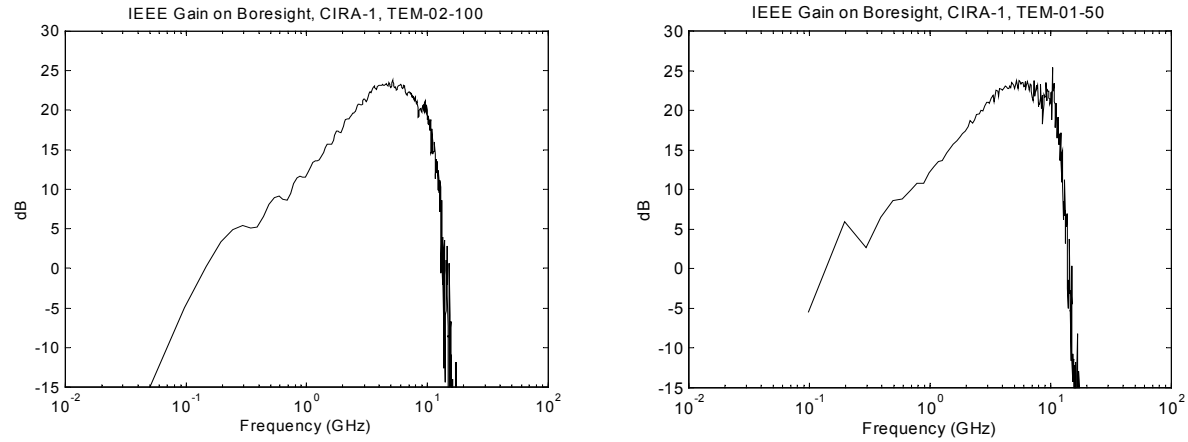

Figure 4.5 IEEE gain of the CIRA on boresight.

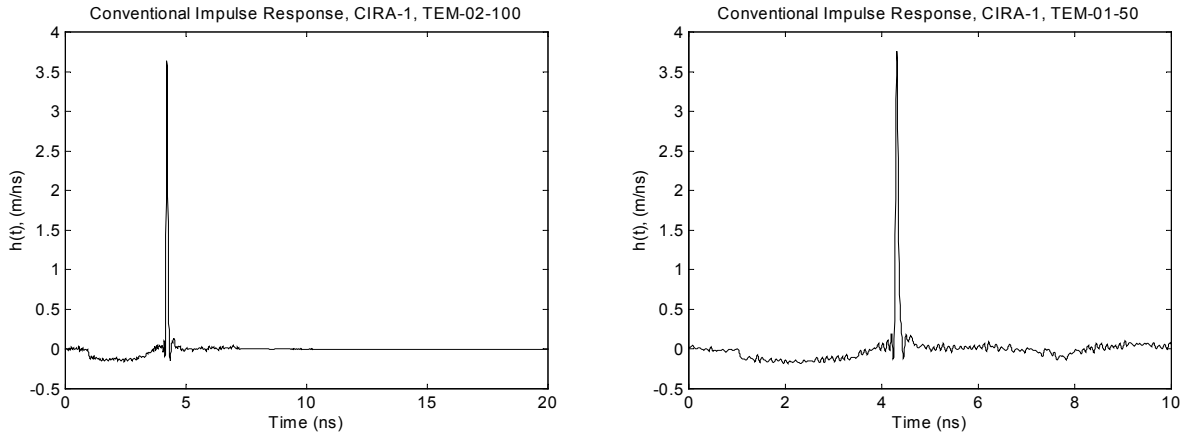

Figure 4.6 Conventional impulse response, $h(t)$ [2]

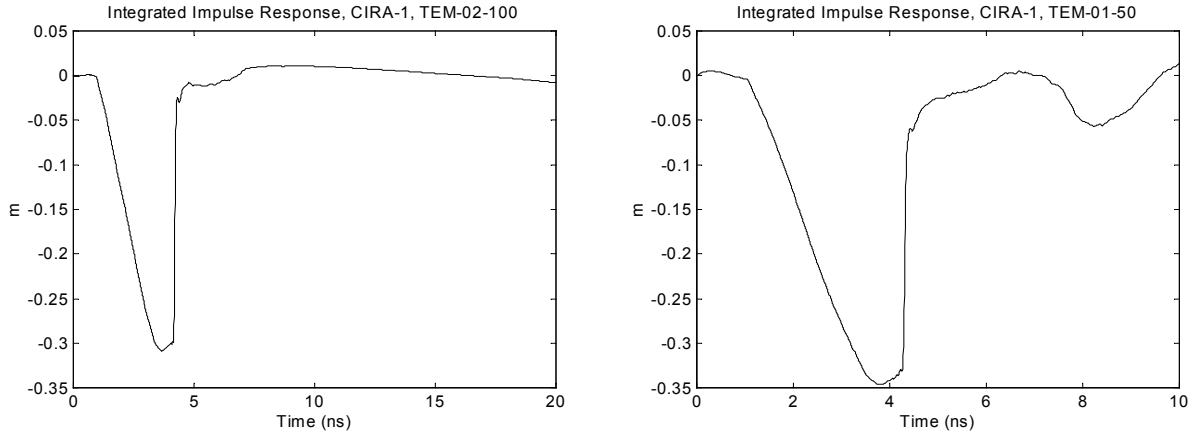

Figure 4.7 Integrated impulse response (h_a = 0.30 m)

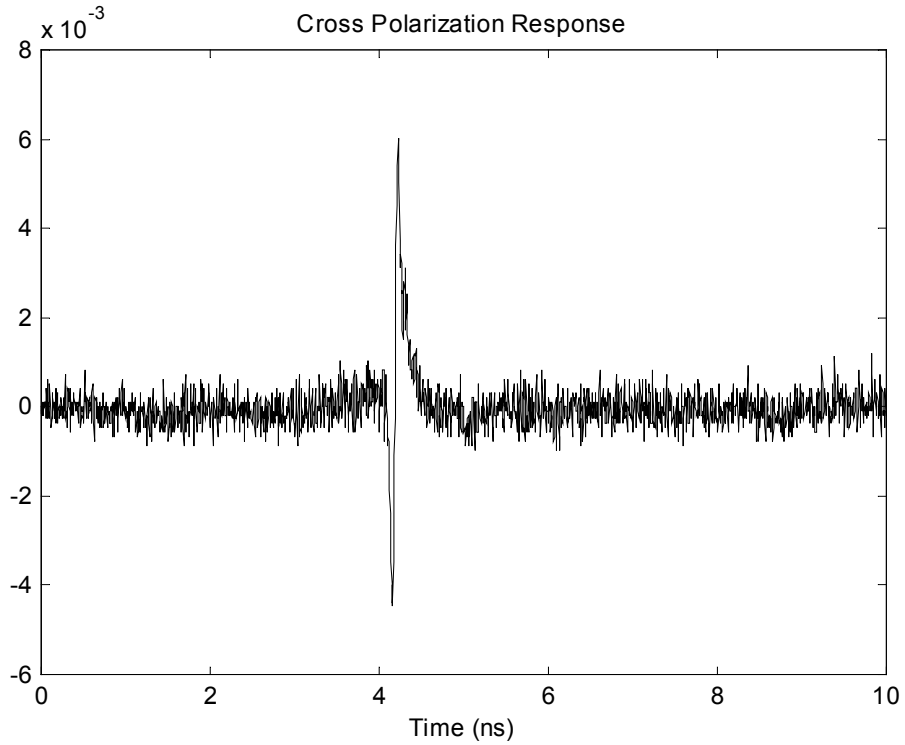

Figure 4.8 Cross polarization response (raw data, zero-padding not shown).

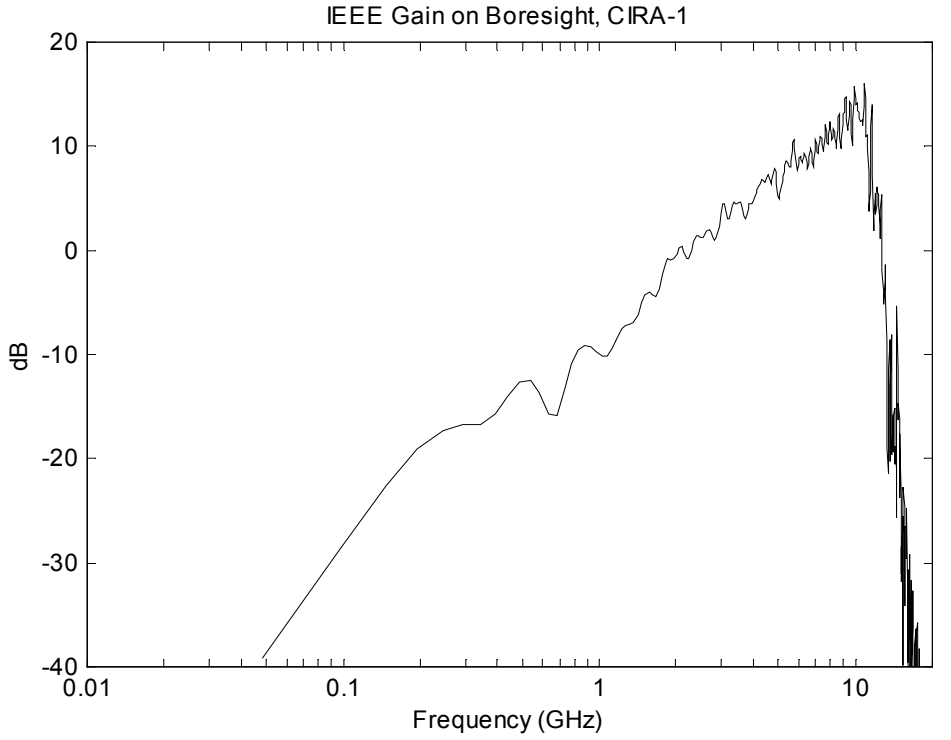

Figure 4.9 IEEE gain of cross polarization response.

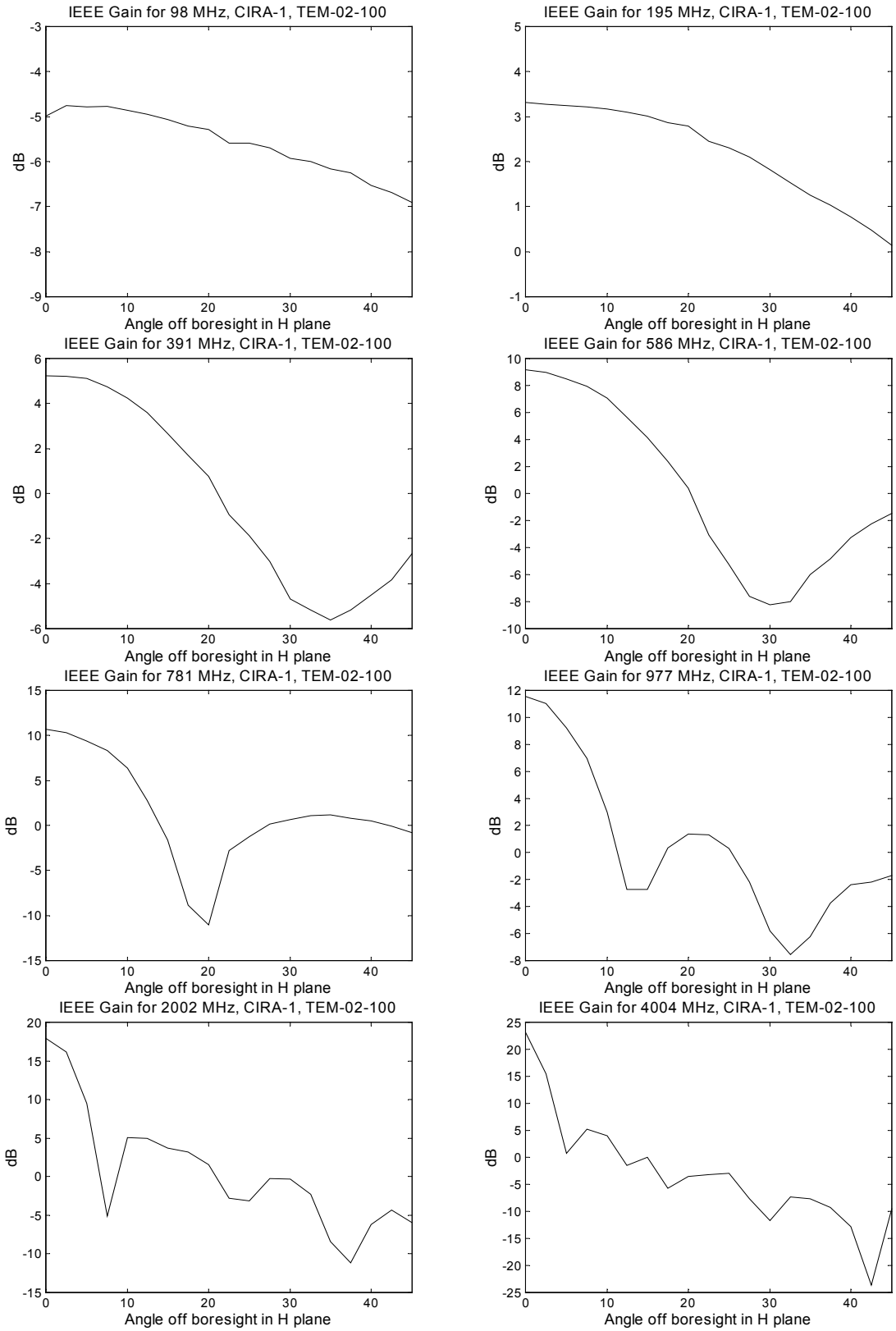

Figure 4.10 IEEE gain vs. angle off boresight in H plane.

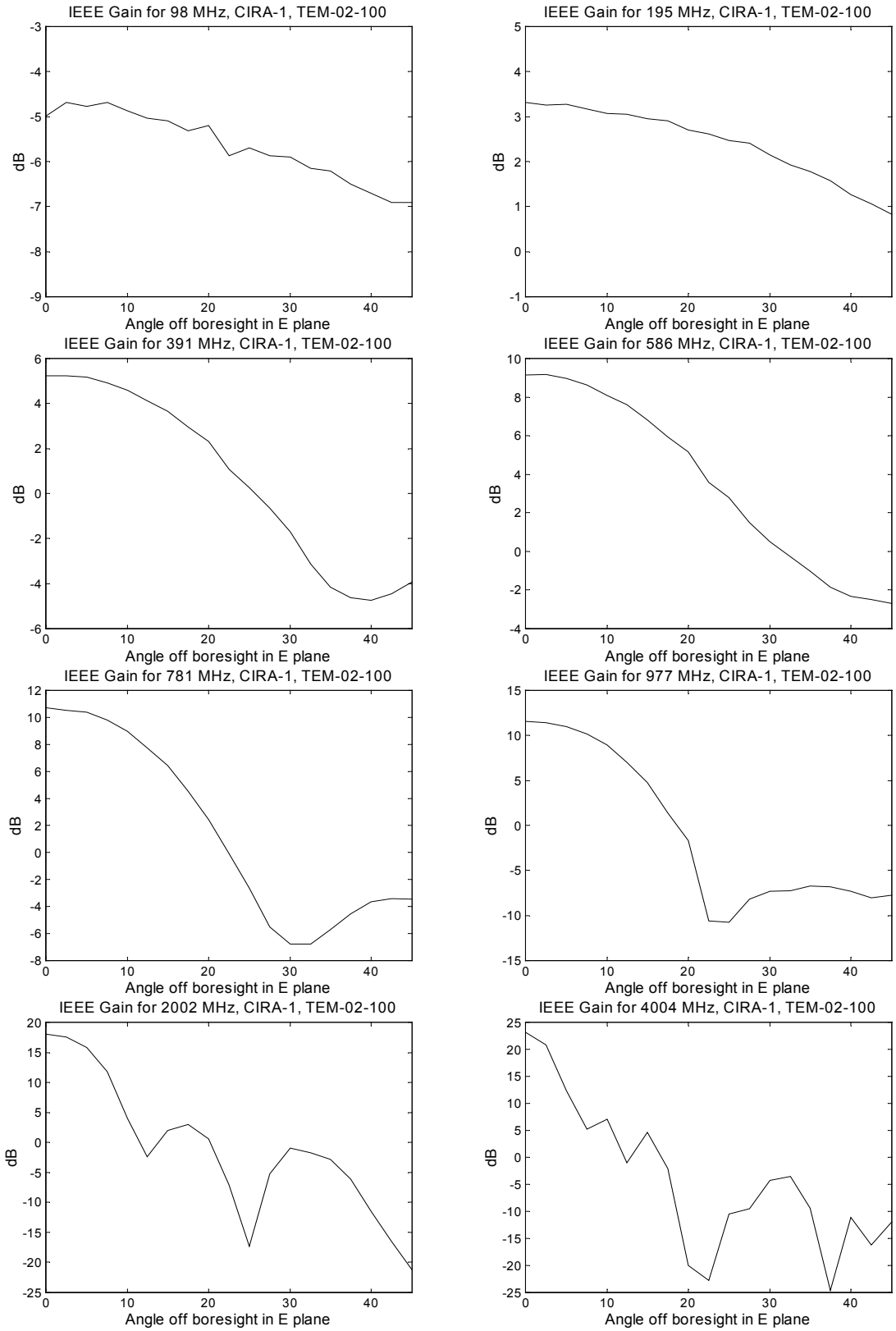

Figure 4.11 IEEE gain vs. angle off boresight in E plane.

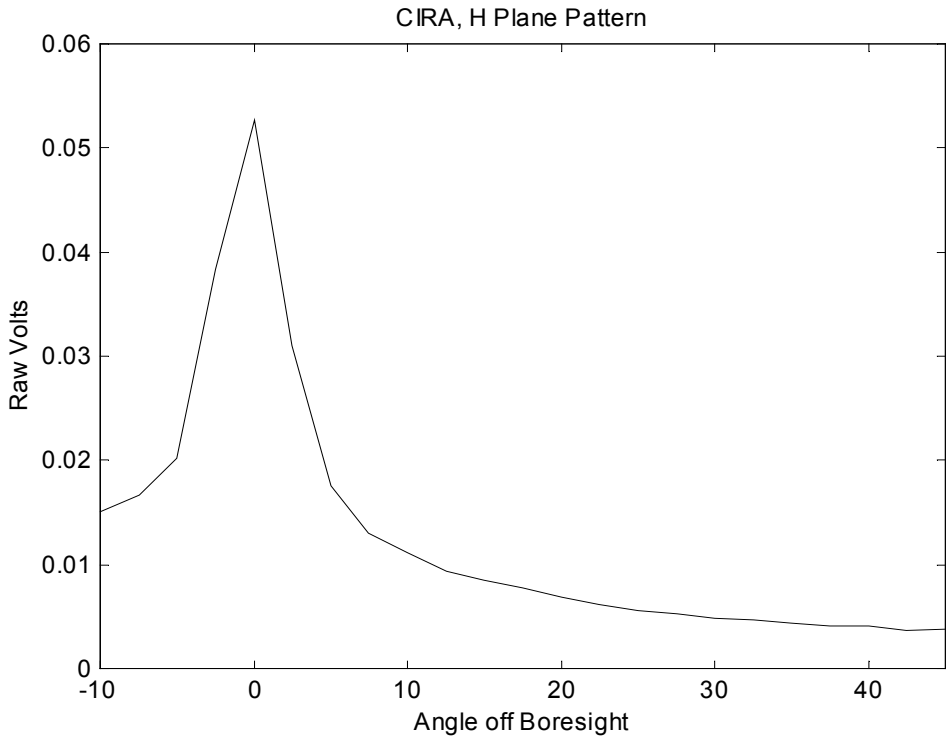

Figure 4.12 Antenna pattern based on peak raw voltage measurements in H plane.

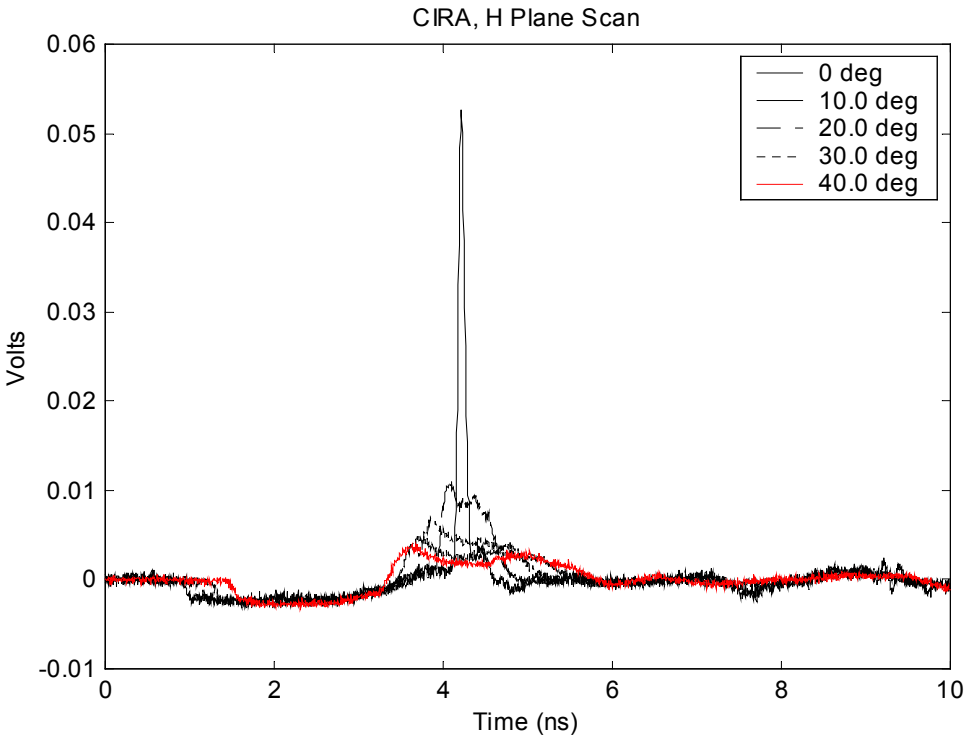

Figure 4.13 Raw voltage at several angles in H plane.

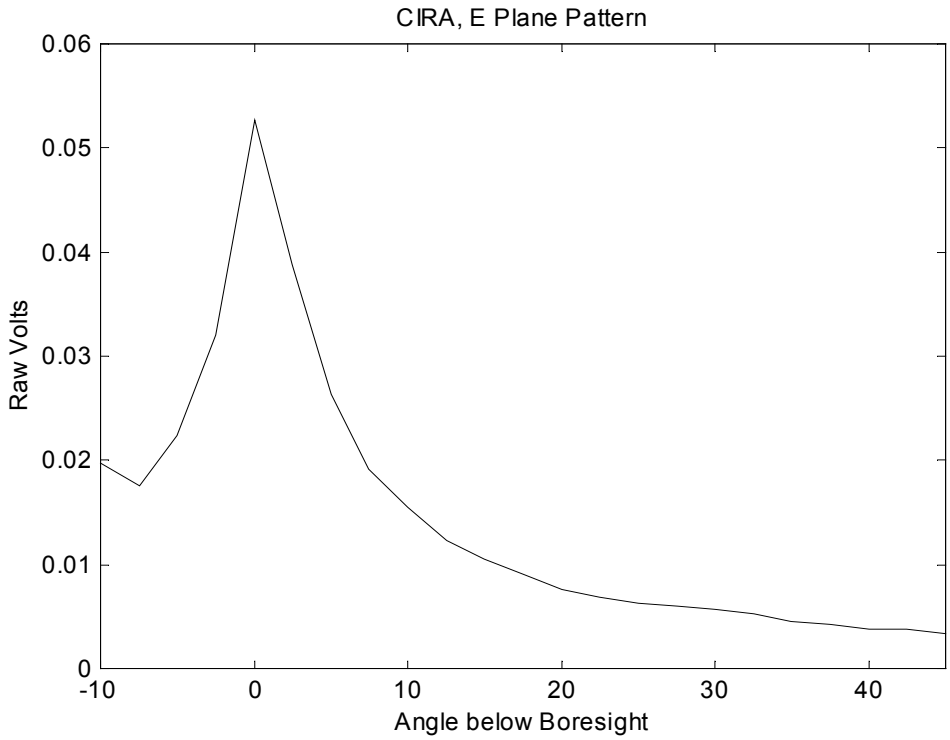

Figure 4.14 Antenna pattern based on peak raw voltage measurements in E plane.

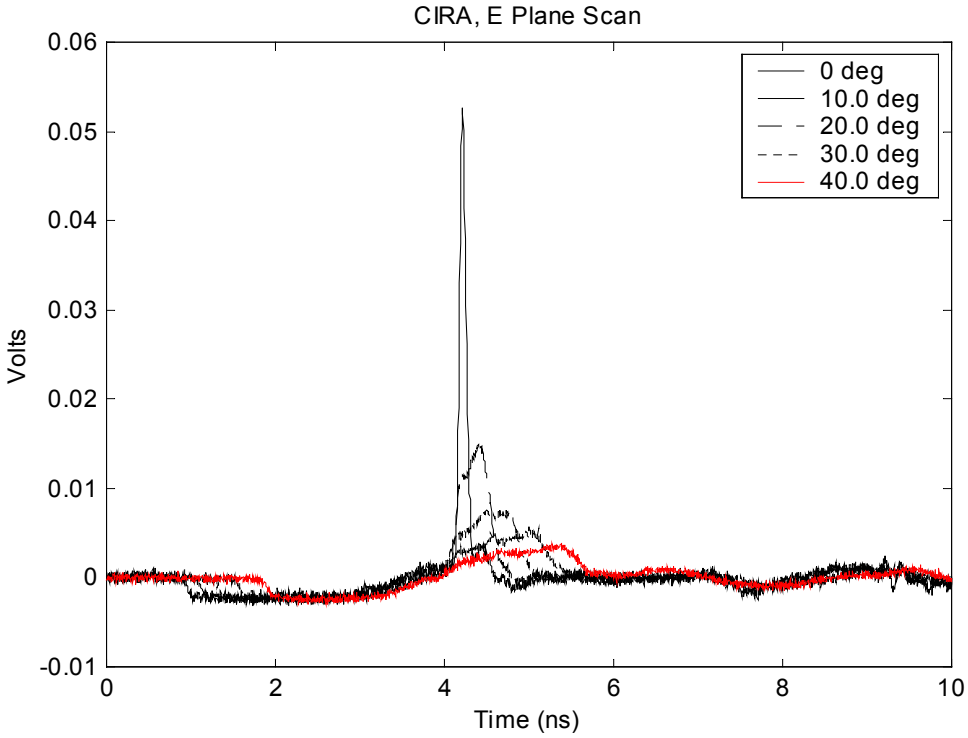

Figure 4.15 Raw voltage measurements at several angles in E plane.

V. Conclusions

The CIRA-1 meets the design requirements for a collapsible, man-portable, 1.22 m (48 in.) diameter IRA. When folded, the antenna is 102 mm (4 in.) in diameter by 0.81 m (32 in.) long and weighs about 2 kg (4.5 lb.). The entire system shown in Figure 3.3 weighs less than 5.5kg (12 lb.). The antenna can be set up in the field by 1 or 2 people and can be attached to a variety of military and COTS transmitters and receivers. The redesigned CIRA is now commercially available from Farr Research, Inc. as model FRI-CIRA-1.

The antenna has an umbrella-like design, with a reflector sewn from a tough conductive mesh fabric. This fabric is very strong, stretch resistant, lightweight, and is has a greatly reduced the wind loading when compared to the rip-stop nylon that was previously used.

The new locking mechanism greatly improved the ease of opening the antenna. The CIRA-1 has a very flat TDR and is usable from below 50 MHz to above 8 GHz. The peak gain is 23 dB at 4 GHz.

Acknowledgements

We wish to thank Dr. Carl E. Baum for helpful comments on this work.

Patent Notice

A patent is pending on the antenna described in this note.

References

1. L. H. Bowen, E. G. Farr, and W. D. Prather, Fabrication and Testing of Two Collapsible Impulse Radiating Antennas, Sensor and Simulation Note 440, November 1999.

2. E. G. Farr and C. E. Baum, Time Domain Characterization of Antennas with TEM Feeds, Sensor and Simulation Note 426, October 1998.

3. L. H. Bowen and E. G. Farr, Recent Enhancements to the Multifunction IRA and TEM Sensors, Sensor and Simulation Note 434, February 1999.

4. J. S. Tyo, Optimization of the Feed Impedance for an Arbitrary Crossed-Feed-Arm Impulse Radiating Antenna, Sensor and Simulation Note 438, November 1999.